Tectono-metamorphic evolution of the Simano-Adula nappe boundary, Central Alps, Switzerland

by *Roger Rütti*[1,2]

Abstract

This paper presents a regional study undertaken in the Penninic zone of the Central Alps in southern Switzerland. The studied region is situated on the boundary of the lower Penninic Simano nappe and Adula nappe. The region is characterized by three major phases of deformation designated D_1, D_2 and D_3, and Post-D_3 sequentially. During phase D_1, the Adula nappe was thrust northwards onto the Simano nappe. Phase D_2 represents the main phase of Alpine metamorphism and deformation under upper amphibolite facies conditions. During this event the nappe boundary was isoclinally folded. The structures due to the deformation phase D_2 represent the dominant structures in the entire region. Phase D_3 corresponds to the backfolding of the Alpine nappe pile. This deformation phase is only locally preserved in the study region. Post-D_3 deformation is a brittle deformation of the Alpine nappes under greenschist facies conditions. P-T calculations were carried out using different calibrations of the GARB (garnet-biotite) thermometer and the GASP (garnet–aluminosilicate–quartz–plagioclase) barometer. The average P-T conditions obtained for the main metamorphic event D_2 are of about 7 kbar and 625 °C. Metapelites of the Adula nappe complex appear to record high-pressure conditions that they once were subjected to in the Alpine subduction zone during Early Tertiary. The difference of pressure conditions was 2 to 4 kbar relative to the Simano nappe in which metapelites seem to record only the Barrovian-type metamorphism of the Central Alps.

Keywords: deformation, metamorphism, Simano nappe, Adula nappe, Central Alps.

1. Introduction

This paper presents a regional study undertaken in the Penninic zone of the Central Alps in southern Switzerland in a region situated on the boundary of the lower Penninic Simano nappe and Adula nappe. In this region, covering roughly 10 km² (Figs 1 and 2), Mesozoic metasediments, generally regarded as the nappe separator in the Central Alps, are completely missing. The metamorphism is of amphibolite facies conditions and the silimanite-in isograd crosscuts the field area (Fig. 1; THOMPSON, 1976).

1.1. ADULA NAPPE COMPLEX

The Adula nappe complex, within the lower Penninic zone of the Central Alps is formed by the Adula nappe sensu stricto to the east and the Cima Lunga unit to the west (Fig. 1). It consists predominantly of pre-Mesozoic basement rocks interlayered with some basic and ultrabasic bodies, marbles and quartzites. For the marbles and quartzites, occurring as thin slices interleaving with pre-Mesozoic basement lithologies and also known as "internal Mesozoic" (PROBST, 1980), a Triassic sedimentation age is postulated (JENNY et al., 1923). In the north, Mesozoic metasedimentary rocks of the Misox zone separate the Adula nappe complex from the overlying middle Penninic Tambo nappe. In the footwall the metasediments of the Soja zone separate the underlying Simano nappe from the Adula nappe. These metasediments unambiguously define the nappe boundary between Olivone and Pizzo di Claro (Fig. 1). Further to the south this contact becomes ambiguous. Alpine mid-Tertiary Barrovian-type regional metamorphism has overprinted the Adula nappe complex with isograds cross-

---

[1] Department of Earth Sciences, University of Lausanne, Switzerland.

[2] Present address: Department of Earth Sciences, Institute of Mineralogy and Petrography, ETH-Zentrum, CH-8092 Zürich, Switzerland. <roger.ruetti@erdw.ethz.ch>
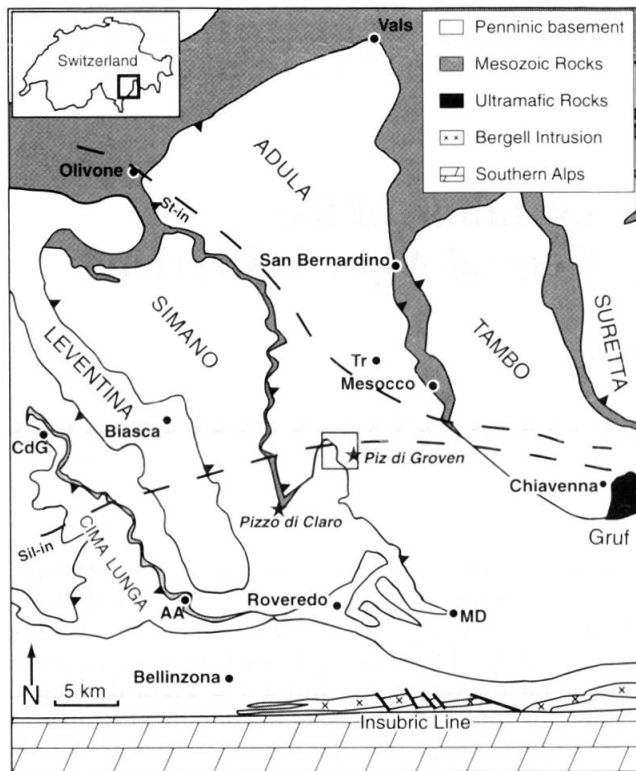
Fig. 1 Tectonic map of the Central Alps of Switzerland modified after HEINRICH (1983). The study area is marked by a square. Sillimanite-in isograd (Sil-in) is taken from THOMPSON (1976), the Staurolite-in isograd (St-in) from NIGGLI and NIGGLI (1965). (AA = Alpe Arami, CdG = Cima di Gagnone, MD = Monte Duria, Tr = Trescolmen)

cutting the nappe boundaries (Fig. 1; FREY et al., 1980; HEINRICH, 1986). Metamorphic grade increases from middle greenschist facies, in the Bündnerschiefer and northern Adula nappe (KUPFERSCHMID, 1977), to upper amphibolite facies, in the southern Adula nappe (KLEIN, 1976a, b; KOCH, 1982; HEINRICH, 1986) and in the Cima Lunga unit (GROND et al., 1995; PFIFFNER, 1999). This Barrovian-type metamorphism has overprinted an older high-pressure metamorphic event within the Adula nappe complex. The high-pressure event is recognized in meta-ultrabasites, metabasites and metapelites of the Adula nappe complex (e.g. EVANS and TROMMSDORFF, 1978; EVANS et al., 1979; HEINRICH, 1986; MEYRE et al., 1997, 1999; PFIFFNER, 1999) as well as in the internal (VAN DER PLAS, 1959) and external Mesozoic rocks (LÖW, 1987). The grade of the high-pressure metamorphic event increases from north to south with conditions of 450–550 °C and 10–13 kbar at Vals (blueschist facies) and 750–900 °C and 18–35 kbar at Trescolmen (eclogite facies; MEYRE et al., 1997; PARTZSCH, 1998). High-pressure conditions for this event further to the south at Alpe Arami, Monte Duria and Cima di Gagnone are in the

range of 750–800 °C and 25–30 kbar (Fig. 1; MÖCKEL, 1969; ERNST, 1978; EVANS and TROMMSDORFF 1978; EVANS et al., 1979, 1981; HEINRICH, 1986; NIIDA and GREEN, 1999; NIMIS, 1999).

Sm–Nd ages of garnets in eclogites in the Cima di Gagnone region by BECKER (1993) and U–Pb SHRIMP-data of zircon rims of garnet-peridotites and garnet-pyroxenites at Alpe Arami (GEBAUER, 1996) give concurring Eocene ages of 45–40 Ma for the maximum pressure of the Cima Lunga unit.

The age of the Adula nappe eclogites is controversial. BECKER (1993) describes a Sm–Nd garnet-clinopyroxene-whole rock isochron for an eclogite at Trescolmen showing an age of 92.5 ± 7.2 Ma. A Cretaceous formation age of eclogites is sometimes assumed (HUNZIKER et al., 1989; STECK and HUNZIKER, 1994; SANTINI, 1993), but a Tertiary age is not excluded (SANTINI, 1993). SCHMID et al. (1996) prefer a Tertiary age for the high-pressure metamorphism based on stratigraphic and structural arguments. BIINO et al. (1997) postulate a pre-Alpine age, perhaps even Hercynian, for the metamorphism of eclogitic rocks in the Adula nappe as well as those of the Cima Lunga unit. If the high-pressure event is of Alpine age, it is restricted to the Adula nappe complex, as maximum pressure conditions in the underlying Simano nappe range up to 12 kbar (IROUSCHEK, 1983). The eclogites of the overlying Tambo and Suretta nappes are of a pre-Alpine age (BAUDIN et al., 1993; MARQUER et al., 1996) and maximum pressures range between 11 and 13 kbar (NUSSBAUM et al., 1998).

The structural evolution of the Adula nappe complex during the high-pressure metamorphic event and the subsequent Alpine history has been studied by several researchers (BAUMGARTNER and LÖW, 1983; LÖW, 1987; MEYRE and PUSCHNIG, 1993; GROND et al., 1995; PARTZSCH, 1998; MEYRE et al., 1997; PFIFFNER, 1999).

1.2. SIMANO NAPPE

The Simano nappe forms a large basement nappe in the Central Alps (Fig. 1) covering much of the area of the broad Lepontine "metamorphic dome". A metagranitic body forms the core of the nappe (JENNY et al., 1923; DAL VESCO, 1953; KELLER, 1968; CODONI, 1981). The upper parts of the nappe mainly consist of pre-Mesozoic metapelitic gneisses and mica schists, intercalated with some amphibolites. Ultramafic rocks are uncommon (DAL VESCO, 1953). Cordierite-bearing rocks of unknown origin (IROUSCHEK, 1983), micaschists and paragneisses with multiple generations of
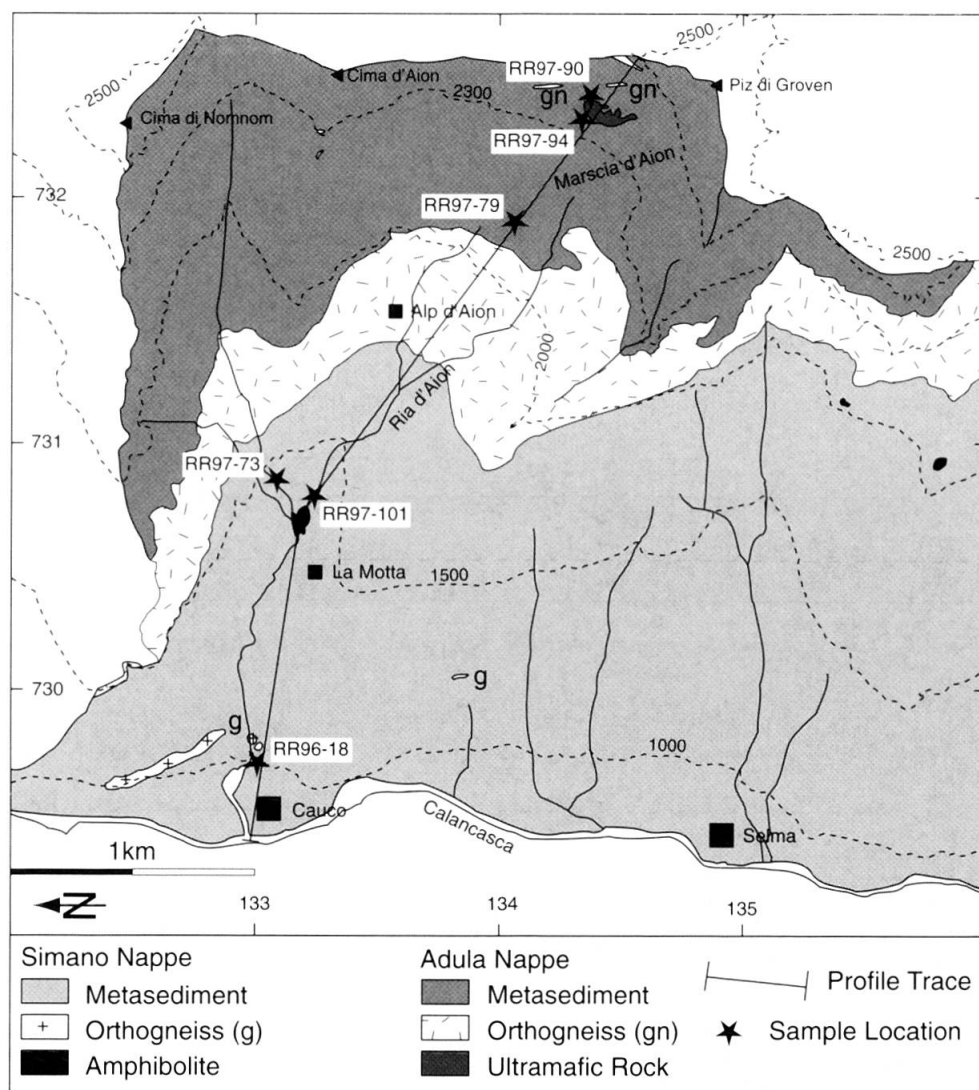
Fig. 2 Detailed geological map of the study area. Stars represent the samples used for thermobarometry and are indicated also on the profile of figure 3.

garnet, staurolite and kyanite, and amphibolites with zoned garnet, hornblende and plagioclase (GRANDJEAN et al., 1999), indicate a complex polyphase metamorphic history. Evidence of early Alpine history has been largely obliterated by the main phase of Alpine metamorphism (FREY et al., 1976). The metamorphism gradually increases from lower amphibolite facies conditions in the northern Simano nappe to upper amphibolite facies conditions in the southern parts. ENGI et al. (1995) and TODD and ENGI (1997) estimate P-T conditions of the main phase of Alpine metamorphism to 5–6 kbar and 500–600 °C. IROUSCHEK (1983) reports metamorphic pressures of up to 12 kbar in metapelites of the Simano nappe. More details on the metamorphism are given by CODONI (1981), FREY et al. (1974, 1976, 1980), KELLER (1968), KLEIN (1976a, b) and KOCH (1982). No evidence for a high-pres-

sure metamorphic event equivalent to the one occurring in the Adula nappe has been found in the Simano nappe so far.

The Simano nappe is separated from the underlying Leventina gneiss by locally observed Mesozoic metasedimentary rocks (Triassic quartzites, NIGGLI et al., 1936). The Mesozoic rocks of the Soja zone extending to the Pizzo di Claro (Fig. 1) separate the Simano nappe from the overlying Adula nappe complex. Further to the south, the nappe boundary becomes ambiguous.

Early studies outline some aspects of the structural evolution of the Simano nappe (KELLER, 1968; AYRTON and RAMSAY, 1974; CODONI, 1981). However, modern techniques of structural geology have only been applied to small parts of the Simano nappe (e.g. western parts of the Campo Tencia subunit by GRUIJIC and MANCKTELOW, 1996).
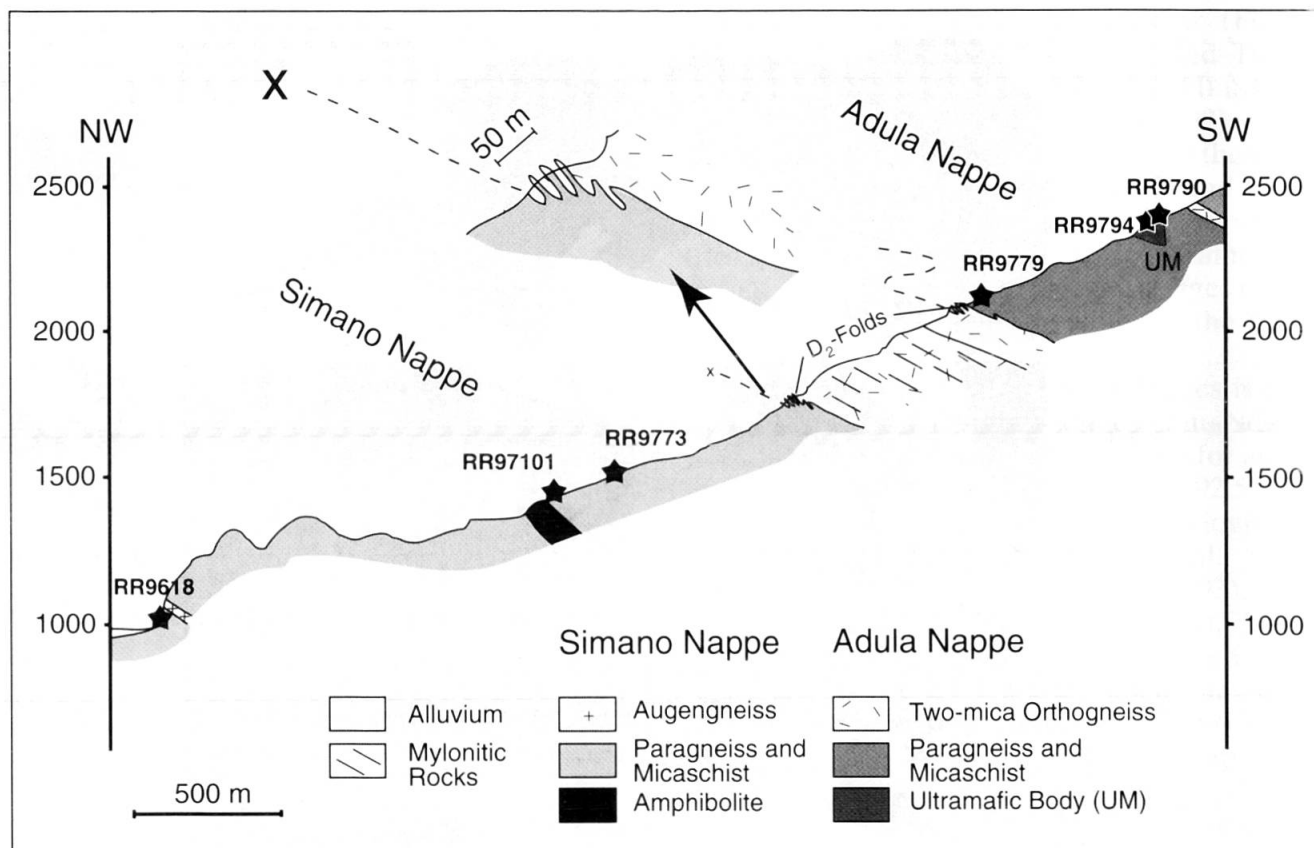
Fig. 3 Section A–B across the study area is shown with an enlargement of the contact zone. For location of the section see figure 2. Stars represent the outcrops of the samples used for thermobarometry.

This work investigates the structural relationships of the Simano and Adula nappes. Of particular interest is the behavior of the two units in their boundary zone, as it is not rigorously defined as further to the west or north (Fig. 3). An additional goal of this study is to establish whether traces of the high-pressure metamorphism event are found in this region with predominantly metapelitic, semipelitic and paragneissic lithologies. The study of fabrics in thin section as well as the determination of the white mica-polytype were undertaken to address this question. Finally, thermobarometric techniques were applied in this study to elucidate the metamorphic conditions across the nappe boundary.

2. Structures

The structural elements observed in the field both for the Simano and the Adula nappes are ascribed to three phases of ductile and one phase of late brittle deformation. Figure 4 shows stereographic projections summarizing the field measurements of the structural elements. The folding style of the different deformation phases encountered in the field is outlined in figure 5.

2.1. DEFORMATION PHASE D_1

Thrusting of the Adula nappe onto the Simano nappe most probably led to the generation of folds (D_1-folds) observed on outcrop scale. These folds are manifest by intensely deformed quartz veins or veinlets and cannot be assigned to any subsequent deformation phase. The subsequent deformation phase D_2 has overprinted the D_1-folds, with D_1 and D_2 fold axes lying parallel to each other (Fig. 5). On a microscopic scale, the deformation phase D_1 can be recognized by an oblique orientation of white mica inclusions in quartz and feldspar compared to the main foliation S_2 of both nappes. These inclusions enclose an angle of about 60° with S_2.

2.2. DEFORMATION PHASE D_2

The second deformation phase D_2 generates the dominant structures in both nappes of the studied area. The main foliation S_2 has a monotonous and homogeneous dip to the NE. S_2 and a series of flat lying folds with fold axes F_2 parallel to the stretching lineation L_2 characterize this deformation phase.
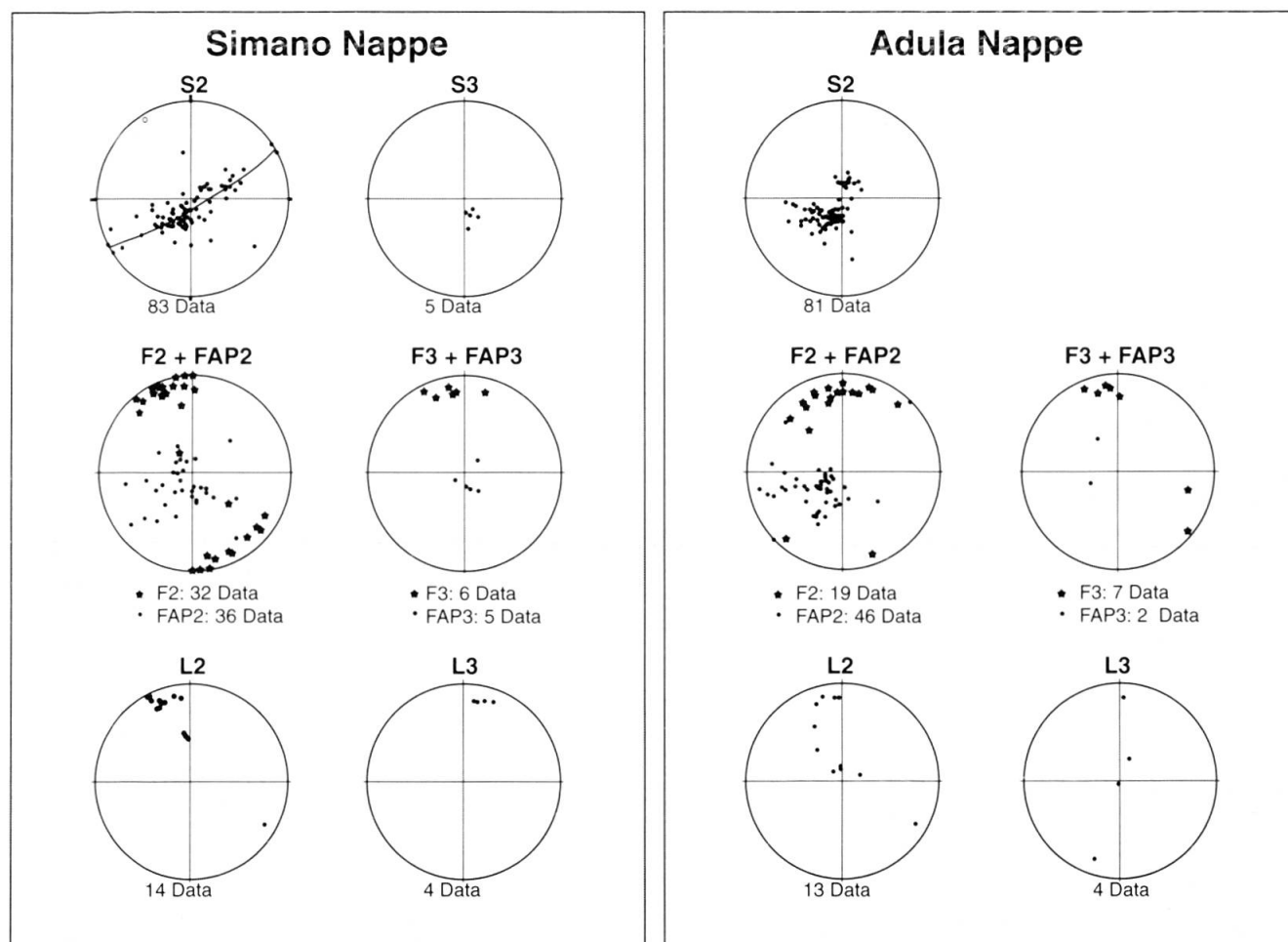
Fig. 4 Equal area stereographic projections (lower hemisphere) of the structural elements measured in the Simano and Adula nappes.

Large macroscopic D_2-folds (scale up to several hundreds of meters) are only rarely observed (Fig. 3). D_2 probably formed isoclinal folds on all scales with fold axes oriented in a NNW direction. On the mesoscopic scale these folds are isoclinal similar folds of type 3 after RAMSAY and HUBER (1987) (Fig. 5).

The same type of fold is observed at the contact of the two nappes, where paragneisses of the Simano nappe are isoclinally folded over a thickness of about 50 m (metric folds) with the two-mica orthogneiss occurring at the base of the Adula nappe (Fig. 3). The two-mica orthogneiss displays a mylonitic fabric that is not observed in the upper part of this lithology. No other mylonites were observed in the study area. The mylonite represents the contact between the two nappes and it represents the extension of the contact in the metasedimentary rocks (metacarbonates) observed further to the west and to the north (SPICHER, 1980; CODONI, 1981).

In stereographic projection the main schistosity S_2 defines a great circle (best fit: 330/09) for the Simano nappe (Fig. 4). This observation is indica-

tive of subsequent overprinting by D_3. Figure 4 shows that the fold axes F_3 are parallel to the pole of this great circle. In the Adula nappe the scatter of the S_2-values is larger (best fit: 315/01).

In the Simano nappe the fold axes F_2 are plunging in a NW to N direction (mean value: 354/14). In the Adula nappe these fold axes show a greater variation from NW to NE, but the mean value remains the same (351/19). The fold axial planes FAP_2 dip in a NE direction in both nappes with the same degree of scatter (mean value: Simano 352/12; Adula 001/19).

Stretching lineation L_2 (quartz and feldspar) in both nappes points in a NNW direction with larger dips in the Adula nappe (mean values: Simano 344/21; Adula 348/41). The measured values of L_2 show a large variation of dip.

In thin section, S_2 is outlined by micas and quartz and feldspar-rich bands in metapelites and semipelites. In amphibolites, micas and hornblende are oriented along S_2. Mica fish and shear bands, which can be assigned to D_2, show a "top-to-the-north" shear sense in both nappes.

2.3. DEFORMATION PHASE D_3

As the field region is situated in the limbs of the two nappes, the deformation phase D_3 is not as penetrative as deformation phase D_2. As a consequence, D_3 is only rarely preserved in the field and is almost imperceptible in outcrops. On a mesoscopic scale the deformation phase D_3 has locally folded features of D_2 (Fig. 5). Larger features have not been observed.

D_3 is characterized by a crenulation foliation S_3 with a mean value of 277/08 in the Simano

Fig. 5 Deformation style during D_2 and D_3 as observed within amphibolites, metapelites and paragneisses with relict structures of older deformation phases (D_1). a) D_2-fold in a paragneiss of the Simano nappe. b) D_2-folds in a metapelite of the Adula nappe. c) D_3-folds as found in both nappes. Note that the folding style occurs at all scales.

nappe. The fold axial planes FAP_3 of the two nappes are essentially parallel to each other (mean values: Simano 291/07, Adula 276/23). The fold axes F_3 are oriented along an N–S direction (mean values: Simano, 351/15; Adula, 013/16). The folds are similar folds of type 2 after RAMSAY and HUBER (1987) with an open interlimb angle. Stretching lineations L_3, mainly of elongated quartz, show the same direction (mean values: Simano, 014/17; Adula, 013/48), but the dip values show a larger scatter in the Adula nappe. The structural elements of this deformation phase (S_3, F_3, FAP_3, L_3) show the same orientations in both the Adula and Simano nappe.

D_3-features are only observed in metapelites and semipelites. In thin sections micas (biotite and muscovite) outline the deformation in these rocks. The microlithons due to D_3 are formed by recrystallized mica.

2.4. POST-D_3 DEFORMATION PHASE

A late phase of brittle deformation fractured all lithologies at all scales. This fracturing, oriented roughly in an E–W direction, can be traced throughout the Central Alps.

Cataclastic rocks and gouges, which show a greenschist facies metamorphism, are found along large fractures crosscutting the entire field region. The displacement along these fracture planes could not be determined because fault tracers (displaced horizons) in the monotonous and homogenous lithologies of the field area are difficult to interpret.

2.5. DISCUSSION

The structural elements measured in both the Simano and the Adula nappes show the same orientation during the deformation phases D_2 and D_3 (Fig. 4). This suggests that the Simano and the Adula nappes have a common history that started with D_2, and most probably commenced when they were thrust on each other. The folded contact of the two nappes shows that the nappes were already bound together during D_2. It is suspected, that the few signs of deformation phase D_1 reflect the thrusting of the Adula nappe onto the Simano nappe.

Comparing the orientation of the measured structural elements of deformation phases D_1 to D_3/post-D_3 with the literature (AYRTON and RAMSAY, 1974; BAUMGARTNER and LÖW, 1983; LÖW, 1987; MEYRE and PUSCHNIG, 1993; GROND et al., 1995; PARTZSCH, 1998; MEYRE et al., 1997;
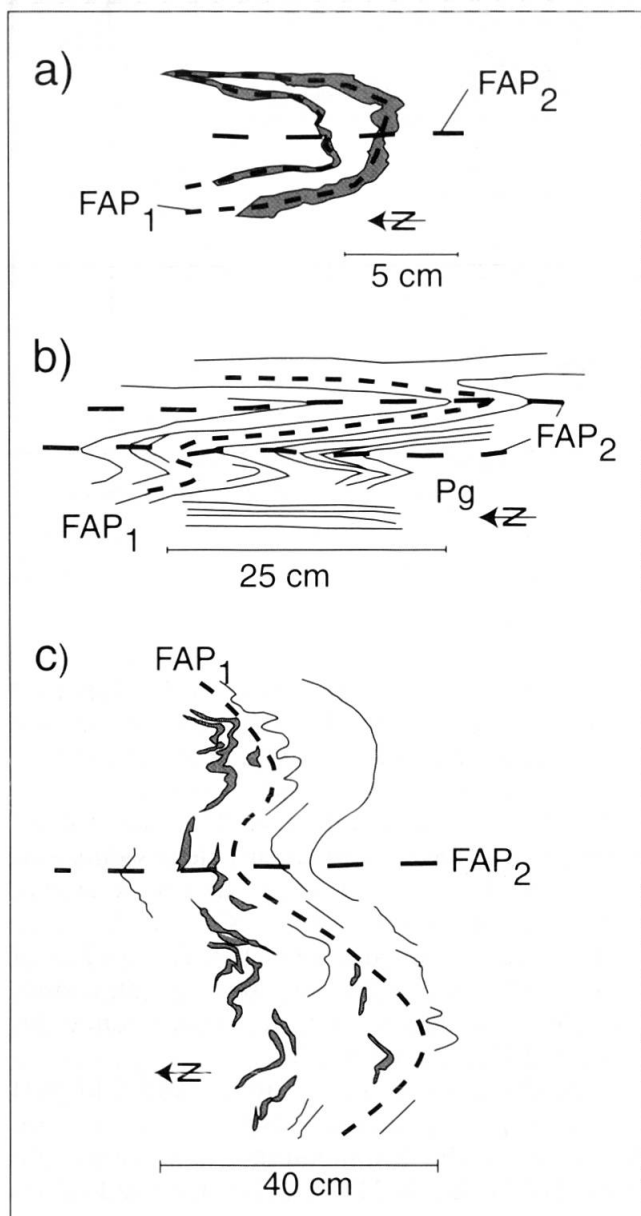
PFIFFNER, 1999) no orientation of structural elements corresponding to the high-pressure event is observed in either nappe which is consistent with the earlier studies. The comparison also shows that the measurements of this study are consistent with previous studies.

KÜNDIG (1926) noted the difficulty of defining the nappe boundary in the study region, because of the lack of Mesozoic metasediments. According to KÜNDIG (1926), the boundary is defined by the presence of shear zones, fault planes and breccias as well as by the folding of the footwall and the presence of metabasites, micaschists and paragneisses. The present work confirms his observations (Fig. 3).

After PARTZSCH (1998) the basal contact of the Adula nappe with the Simano nappe is sharp and accompanied by a mylonitic zone. He postulates that this basal thrust plane truncates large-scale isoclinal D_2-folds with E–W oriented fold axes of the Simano nappe. The dominant structures are generated by the deformation phase D_3 with lineations pointing NW. This work identified metric shear zones in the Simano nappe below the contact zone. Although the shear zones cut isoclinal D_2-folds, they do not represent the thrusting because the structural elements of the two units show the same orientation indicating a common history that began before D_2. These observations suggest that the thrusting occurred before D_2 as the contact zone is folded, whereas PARTZSCH (1998) assigns thrusting to D_2.

3. Metamorphism

3.1. ROCK TYPES AND MINERAL ASSEMBLAGES

The studied region consists of paragneisses, meta-semipelites and metapelites interlayered with some amphibolites and orthogneisses (Figs 2 and 3). An ultramafic body is situated at an altitude of 2350 m in the Adula nappe (Figs 2 and 3).

The *orthogneisses* are massive with a variable thickness of 5 to 20 m in the Simano nappe. The orthogneisses of the Adula nappe form the rock type in and above the contact zone of the two nappes as well as thin layers in the upper part of the area (Figs 2 and 3). The mineral assemblage is Qtz + Kfs + Pl + Bt + Ms (mineral abbreviations after KRETZ, 1983). In the Simano nappe these rocks frequently show augen textures with eyes measuring up to several centimeters. The eyes are formed by recrystallized potassic feldspar and are monocrystalline. According to KORNPROBST (1994) monocrystalline eyes can be interpreted as feld-spar phenocrysts of a magmatic rock in contrast to polycrystalline eyes which are derived from sediments. The white mica polymorph is consistently $2M_1$ in this rock type in both units. The two-mica orthogneiss of the Adula nappe is mylonitized at its base. The typical mineral assemblage, which is also found in the upper non-mylonitic parts of this rock type (Fig. 3) is Qtz + Kfs + Ms + Bt ± Pl. The minerals are all recrystallized and form an equigranular fabric that shows strong textural indications of a magmatic origin.

Meta-semipelites and paragneisses constitute the dominant lithologies of the two units. They are not easily distinguished from metapelites, especially when the overall grain size is small, as these rocks gradually grade into each other. Two main types of paragneisses can be observed in the field: two-mica paragneiss and biotite-paragneiss. The two-mica paragneiss contains the mineral assemblage Qtz + Pl + Bt + Ms ± Kfs ± Grt. This paragneiss often shows a layering of mica-rich and felsic bands (Qtz, Fsp). The granoblastic fabric has a fine mean grain size (< mm). The qualitative analysis of the white mica polymorph gives the $2M_1$ structural form with a slightly phengitic composition in both nappes. The biotite-paragneiss is characterized by the mineral assemblage: Qtz + Pl + Bt ± Hbl. This rock shows also an alternation of mica-rich and felsic bands. The fabric is granoblastic. The white mica polymorph is the same as in the two-mica paragneiss ($2M_1$).

The *metapelites* in the area have the mineral assemblage Qtz + Pl + Bt + Ms + Ky ± St ± Grt ± Sil ± Gr. Two types of fabric can be observed. One type consists mainly of large prophyroblasts (up to 1 to 1.5 cm) of kyanite and staurolite. The micas (Ms, Bt) are folded around these large arrays of kyanite and staurolite. Garnet is observed only as inclusion in plagioclase, kyanite and staurolite. In the study area this type of fabric only has been observed in the Simano nappe. Characteristic of this fabric is the presence of graphite. It constitutes several volume percent of the rock. It shows microfolds that probably are pre-D_2 as they do not follow the foliation developed in the rock. Furthermore, it has been pushed away by the static growth of kyanite that does not incorporate graphite during its growth. When both kyanite and staurolite are present, their intergrowth is frequent. The second fabric observed is also grano-porphyroblastic containing porphyroblasts of garnet and kyanite which are considerably smaller in size (diameter < cm). Staurolite is present but only in minor amount and its grain size is generally small (< mm). Sillimanite appears as fibrolite and is associated with biotite and garnet. Two generations of garnets show a considerable variation

Tab. 1 Representative mineral analyses (wt%) of garnet, biotite and plagioclase in metapelites used for the GARB and GASP thermobarometry.

Analyses	Simano Nappe												Adula Nappe					
	Sample RR9618			Sample RR97101			Sample RR9773			Sample RR9779			Sample RR9790			Sample RR9794		
	Grt 4-4	Bt 4-1	Plg 2-1	Grt 6-1	Bt 6-1	Plg 1-1	Grt 12-3	Bt 14-1	Plg 11-3	Grt 2-4	Bt 2-3	Plg 2-1	Grt 5-1	Bt 5-1	Plg 3-4	Grt 12-3	Bt 11-1	Plg 11-2
SiO_2	36.78	36.27	61.83	37.58	35.16	62.08	37.02	35.77	63.11	37.07	34.84	62.13	37.64	35.33	62.74	37.04	34.63	64.47
TiO_2	0.02	1.67	n.a.	0.01	1.96	n.a.	0.04	2.05	n.a.	0.04	1.67	n.a.	0.07	2.31	n.a.	0.02	1.91	n.a.
Al_2O_3	20.77	20.16	23.51	20.84	19.31	23.80	20.75	19.62	22.82	20.65	19.43	23.75	20.67	19.41	23.75	20.39	18.65	22.51
Cr_2O_3	0.03	0.02	n.a.	0.03	0.11	n.a.	0.04	0.09	n.a.	0.03	0.05	n.a.	0.03	0.07	n.a.	0.03	0.03	n.a.
FeO*	34.88	18.09	0.07	33.80	18.70	0.08	34.66	17.48	0.00	34.42	20.63	0.08	34.68	19.67	0.29	34.84	21.36	0.00
MnO	2.66	0.10	n.a.	1.06	0.02	n.a.	3.11	0.08	n.a.	1.36	0.07	n.a.	0.70	0.10	n.a.	4.49	0.19	n.a.
MgO	3.43	9.66	n.a.	4.03	9.36	n.a.	3.12	10.08	n.a.	3.44	9.53	n.a.	4.34	9.22	n.a.	2.33	9.28	n.a.
K_2O	n.a.	9.88	0.11	n.a.	8.63	0.14	n.a.	9.34	0.11	n.a.	9.58	0.14	n.a.	9.43	0.13	n.a.	8.78	0.13
Na_2O	n.a.	0.46	9.00	n.a.	0.71	8.70	n.a.	0.31	9.46	n.a.	0.22	8.94	n.a.	0.25	9.07	n.a.	0.30	9.77
CaO	1.75	n.a.	4.81	2.99	n.a.	5.12	1.95	n.a.	3.98	3.35	n.a.	4.91	2.39	n.a.	4.83	1.63	n.a.	3.57
Total	100.32	96.31	99.33	100.35	93.96	99.93	100.69	94.82	99.48	100.37	96.02	99.95	100.53	95.78	100.81	100.77	95.12	100.45
Cations per formula unit**																		
Si	2.951	5.585	2.760	2.990	5.526	2.754	2.965	5.550	2.804	2.962	5.387	2.756	2.990	5.479	2.762	2.985	5.391	2.832
Al^{IV}	0.049	2.415	1.237	0.010	2.474	1.245	0.035	2.450	1.195	0.038	2.613	1.242	0.010	2.521	1.232	0.015	2.609	1.165
Al^{VI}	1.915	0.000	0.000	1.944	1.102	0.000	1.923	1.138	0.000	1.907	0.927	0.000	1.925	1.027	0.000	1.922	0.813	0.000
Ti	0.001	0.193	0.000	0.001	0.232	0.000	0.002	0.239	0.000	0.003	0.194	0.000	0.004	0.270	0.000	0.001	0.224	0.000
Fe^{3+}	0.129	0.000	0.000	0.063	0.000	0.003	0.104	0.000	0.000	0.124	0.000	0.000	0.073	0.000	0.000	0.088	0.000	0.000
Cr	0.002	0.003	0.000	0.002	0.013	0.000	0.002	0.011	0.000	0.002	0.006	0.000	0.002	0.008	0.000	0.002	0.004	0.000
Fe^{2+}	2.212	2.330	0.000	2.186	2.457	0.000	2.217	2.269	0.000	2.176	2.667	0.003	2.230	2.550	0.011	2.260	2.780	0.000
Mn	0.181	0.014	0.000	0.072	0.003	0.000	0.211	0.010	0.000	0.092	0.010	0.000	0.047	0.013	0.000	0.306	0.026	0.000
Mg	0.410	2.217	0.000	0.478	2.193	0.000	0.373	2.333	0.000	0.410	2.196	0.000	0.514	2.133	0.000	0.280	2.153	0.000
K	0.000	1.940	0.006	0.000	1.731	0.008	0.000	1.850	0.006	0.000	1.890	0.008	0.000	1.866	0.007	0.000	1.743	0.007
Na	0.000	0.137	0.780	0.000	0.216	0.749	0.000	0.093	0.815	0.000	0.065	0.769	0.000	0.074	0.774	0.000	0.089	0.832
Ca	0.150	0.000	0.230	0.255	0.000	0.243	0.167	0.000	0.189	0.287	0.000	0.234	0.204	0.000	0.228	0.141	0.000	0.168
Molar fractions																		
X_{Fe}	0.749	0.388	-	0.731	0.410	-	0.747	0.379	-	0.734	0.445	-	0.745	0.426	-	0.757	0.464	-
X_{Mn}	0.061	0.002	-	0.024	0.000	-	0.071	0.002	-	0.031	0.002	-	0.016	0.002	-	0.103	0.004	-
X_{Mg}	0.139	0.370	-	0.160	0.366	-	0.126	0.390	-	0.138	0.366	-	0.172	0.356	-	0.094	0.359	-
X_{Ca}	0.051	-	-	0.085	-	-	0.056	-	-	0.097	-	-	0.068	-	-	0.047	-	-
X_{Al}^{VI}		0.207			0.184			0.190			0.155			0.171			0.136	
X_{Ti}		0.032			0.039			0.040			0.032			0.045			0.037	
X_{Ab}			0.767			0.749			0.806			0.761			0.767			0.826
X_{An}			0.227			0.243			0.188			0.231			0.226			0.167
X_{Or}			0.006			0.008			0.006			0.008			0.007			0.007

n.a.: not analyzed.

* all Fe measured as Fe^{2+}.

** Normalizations: Grt - 8 cations, Bt - 14 cations minus K, Na, Ca after Essene (1989), Plg - 5 cations.

in size: from grains measuring 0.1 mm across up to grains measuring several millimeters in diameter. The metapelites contain only the $2M_1$ white mica polymorph.

The reactions that the metapelites encountered during the prograde path observed in thin section are:

Staurolite+Chlorite → Biotite+Kyanite+H_2O (1)

According to SPEAR (1993), this reaction is responsible for the intimate intergrowth of staurolite and kyanite. Some kyanite shows a undulose extinction. The breakdown of staurolite is caused by the reaction:

Staurolite → Garnet+Biotite+Kyanite+H_2O (2)

Staurolite inclusions in garnet are observed permitting the above formulation. This reaction took place early during D_2 as the main D_2-foliation is folded around arrays of Grt + Bt + Ky. The last reaction that can be observed in the thin sections of the field area is the polymorphic transformation of the aluminosilicates:

Kyanite → Sillimanite   (3)

Nests of fibrolite associated with biotite and garnet manifest this transformation as observed by YARDLEY et al. (1990) and SPEAR (1993).

Reaction (2) marks the onset of upper amphibolite facies conditions and can be estimated on the petrogenetic grid of SPEAR and CHENEY (1989) to occur around at 700 °C. A petrogenetic grid (Fig. 6) for the $K_2O–Al_2O_3–FeO–MgO–SiO_2–C–O–H$ system projected through quartz, the stable aluminosilicates, muscovite, graphite and water was calculated with the PERPLEX program of CONNOLLY (1990) and the database of HOLLAND and POWELL (1998). This grid indicates the location of reaction (2) at 650–700 °C with pressures > 7 kbar. The calculations were made assuming the presence of a fluid formed by the equilibration of water and graphite to account for the effect of the presence of graphite in the Simano metapelites. The grid shows also isopleths for biotite and garnet compositions (Chapter 3.2.).

Amphibolites of the Adula nappe occur generally as boudinaged layers. KÜNDIG (1926) observed several continuous amphibolite layers in the Simano nappe. In both nappes the typical paragenesis is Hbl + Pl ± Bt ± Grt. In the Adula nappe amphibolites may contain several weight percent of biotite and garnet. Garnet-bearing amphibolites are unusual in the Simano nappe. Most amphibolites show a strong alteration of the amphibole minerals by chlorite. In the upper part

of the field region, black walls, probably associated with an ultramafic body, can be locally observed.

Ultramafic rocks are found in one massive body (200 m long and 80 m wide) just below the mountain ridge at about 2350 m (Figs 2 and 3). This body has undergone almost complete hydrothermal alteration. It shows a mineral zonation which is characteristic of ultramafic bodies in the Central Alps as described by PFEIFER (1979). The core of the body is only partly affected by the hydrothermal alteration event and consists of the characteristic mineral assemblage Ol ± Tlc. The protolith therefore is supposed to be a dunite. The next zone towards the country rocks contains hydroxylated minerals such as talc and anthophyllite. Beyond this zone, carbonate minerals such as magnesite can be observed in addition to the hydroxylated minerals. The contact of the ultramafic body is formed by amphibolites. Most of the contact zone is hidden under slope debris. In thin section no traces of the initial fabric can be observed due to hydrothermal alteration. Mafic veins, mostly boudinaged and folded, can be observed in the body. These veins are formed by meta-rodingites (Di + Grt), chlorite-felses and amphibolites. The structural elements associated with these veins have no equivalent in the surrounding country rocks.

3.2. MINERAL COMPOSITION

All minerals used in the thermobarometry calculations (GARB thermometer and GASP barometer) were analyzed using the CAMECA Camebax SX50 electron microprobe of the Earth Sciences Department at the University of Lausanne. The electron microprobe is equipped with 5 spectrometers (LiF, PET and TAP crystals) and operates with the XMAS Software. The operating conditions were set at 15 kV, 20 nA for garnet and at 15 kV, 15 nA for biotite and plagioclase. The matrix correction used was PAP of POUCHOU and PICHOIR (1984). Except for the synthetic CrO_2 and $MnTiO_3$, all standards used are natural oxides and minerals. Mineral analyses are normalized on a cation basis for garnet (8) and on a basis of 8 oxygens for plagioclase. Biotite was normalized on a basis of 14 cations minus K, Ca and Na (ESSENE, 1989). Representative electron microprobe analyses of garnet, biotite and plagioclase in the metapelites are given in table 2.

In both nappes two generations of *garnets* are observed. The older generation consists of large, mostly subidiomorphic porphyroblasts, often with skeletal habit. These garnets measure up to 1 cm

Tab. 2 P-T conditions determined in this study compared with P-T estimates of the Adula and Simano nappes found in the literature.

Simano nappe	T (°C)	P (kbar)	Locality	Swiss Coordinates
This study; RR9618	626	5.98	Cauco	729700/133000
This study; RR9773	639	6.27	Pian Conca	730880/132960
ENGI et al, 1995; DS06	606	5.22	Cauco	729350/133350
Adula nappe	T (°C)	P (kbar)	Locality*	
This study; RR9779	640	8.76	Aion de Sora - S Adula	732080/132260
This study; RR9790	669	7.93	Marscia d'Aion - S Adula	732440/131660
ENGI et al., 1995; DS04	791	6.12	Roveredo - S Adula	729700/122230
ENGI et al., 1995; DS05	682	4.38	Roveredo - S Adula	729850/122250
ENGI et al., 1995; B367	706	6.45	Val Grono - S Adula	734900/121600
ENGI et al., 1995; T082a	640	3.88	Val Grono - S Adula	732970/122460
ENGI et al., 1995; T032bI	561	5.37	Pizzo di Cressim - SE Adula	739580/125600

*to this date, no PT-values exist in the literature close to the study area. The values calculated by ENGI et al., 1995 are several of tens of kilometers away from the study area.

in diameter and contain inclusions of quartz, feldspar, staurolite and micas. The main foliation is bent about these garnets indicating crystallization prior to D_2. The younger generation is smaller (< 0.5 cm), inclusion-free and shows in most cases an idiomorphic habit. These garnets are found in the main schistosity, in some cases in the pressure shadows of older garnets and appear to have crystallized during D_2. The chemical composition of this younger generation has been used in the thermobarometric calculations. In both nappes all measured garnets are almandine-rich (70–75 mol%). These compositions are consistent with those predicted to be stable between the staurolite-out reaction and the polymorphic transformation of kyanite to sillimanite (shaded area of Fig. 6). The pyrope content varies between 11 and 15 mol%, the spessartine content between 2 and 7 mol% (Tab. 1). No significant difference in the chemical composition of pre-D_2 and D_2 garnets was observed. Garnet profiles were measured across the large pre-D_2 porphyroblasts (Fig. 7). The profiles show that Adula prophyroblasts are depleted in FeO and CaO and enriched in MnO relative to Simano porphyroblasts. However, the shape of MnO profile is the same: MnO decreases from the rim towards the center with rim compositions remaining constant. The garnets have about the same MgO content in both nappes and show a bell-shaped distribution. The CaO content remains constant as well as rim composition of FeO and MgO in general.

Three generations of *biotite* are observed in most samples. The earliest occurs as inclusions in large grains of plagioclase and garnet. The second generation is aligned with the main schistosity S_2 and is bent about large porphyroblasts of garnet and shows an undulating extinction. The third type of biotite is post-kinematic as it grows obliquely to the main schistosity. In some samples this third generation forms a crenulation schistosity S_3. The D_2 biotites have been used for the calculations reported here. The biotites used in the thermobarometry calculations contain between 17 to 20 wt% of FeO. Titanium is relatively high in these biotites with amounts of up to 2.7 wt% of TiO_2. Biotites have a X_{Mg} which varies between 0.62 and 0.57 (Tab. 2) and plot generally in the same P-T space as the garnets (Fig. 6).

In the samples used for the thermobarometry only a few grains of *plagioclase* were found. These occur in the matrix and are xenomorphic. In some cases, sericitzation of the plagioclase rim is observed. The plagioclase shows an undulating extinction as well as deformed polysynthetic twins. The plagioclase probably grew before D_2. It often shows inclusions of quartz, garnet and biotite. The plagioclase has anorthite content varying between 22 to 28 mol% (Tab.2).

Kyanite is sometimes intergrown with staurolite due to reaction (1). Kyanite is present in variable amounts in the metapelites. In the Simano nappe, it comprises 10–20 wt% of the metapelites and contains numerous inclusions of quartz, feldspar, garnet and biotite. In the Adula nappe, kyanite is somewhat less abundant (5–15 wt%).

3.3. THERMOBAROMETRY

For thermobarometric calculations, rim compositions of garnet-biotite pairs attributed to deformation phase D_2 were combined. Ideally these compositions could represent local equilibrium.
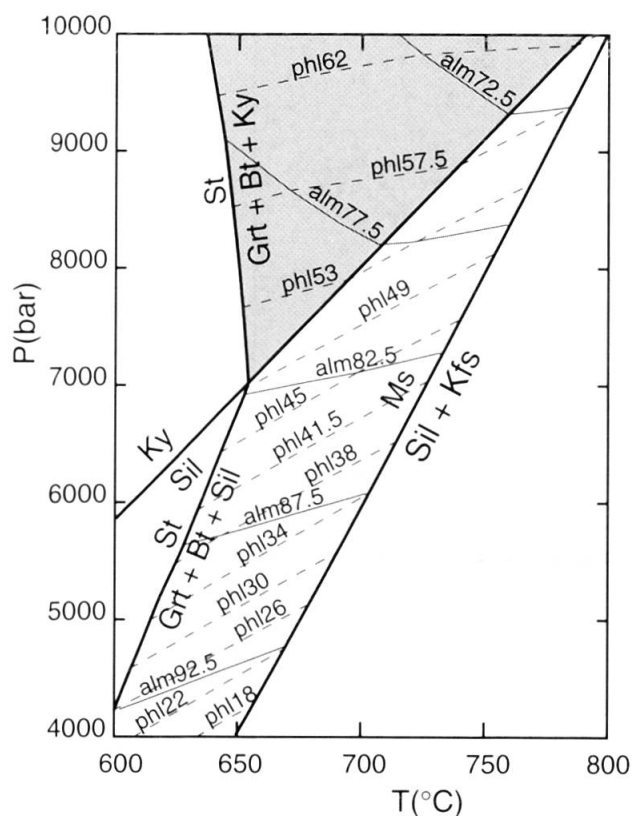
Fig. 6 Petrogenetic grid of the $K_2O-Al_2O_3-FeO-MgO-SiO_2-C-O-H$ system projected through quartz, the stable aluminosilicates, muscovite, graphite and water, generated with the PERPLEX program of CONNOLLY (1990) and the database of HOLLAND and POWELL (1998). The calculations were made assuming the presence of a fluid formed by the equilibration of water and graphite to account for the effect of the presence of graphite in the Simano metapelites. Isopleths of garnet (solid lines) and biotite (stippled lines) are drawn. (alm = almandine-component (Fe) of garnet; phl = phlogopite-component (Mg) of biotite).

No calculations were made with rim compositions of the large porphyroblasts. For barometry, garnet rim compositions were combined with matrix plagioclase rim compositions.

The metapelites of the study area allow the GARB thermometer (garnet-biotite) and of the GASP barometer (garnet–aluminosilicate–quartz–plagioclase) to calculate the pressure and temperatures conditions of the main metamorphic event (D_2).

Garnets of the field area have a MnO and CaO component and these components influence the position of mineral reactions in P-T space (SPEAR 1993). In addition biotites have a rather large amount of Ti (Tab. 2). The thermometers should therefore take into account these effects to yield realistic temperatures. The HODGES and SPEAR (1982) calibration corrects for MnO and CaO in garnet. However, biotite is believed to be-

have ideally, therefore, no correction is made for the Ti-content. The KLEEMANN and REINHARDT (1994) calibration uses the BERMAN (1990) garnet solution model. This model performs even better than the HODGES and SPEAR (1982) model under amphibolite facies conditions according to an evaluation by APPLEGATE and HODGES (1994). KLEEMANN and REINHARDT (1994) use their own model for biotite to account for Ti and Al^{VI}. HOLDAWAY et al. (1997) use their own biotite model and the asymmetric garnet solution model of MUKHOPADHYAY et al. (1993). Figure 8 summarizes the results and the comparison of the three thermometers. The HODGES and SPEAR (1982) thermometer shows a large range of temperature. The KLEEMANN and REINHARDT (1994) formulation as well as the one of HOLDAWAY et al. (1997) constrain the temperature tighter with the former yielding temperatures at the lower temperature boundary and the latter at the upper temperature boundary of the boxes in figure 8.

In the GASP barometer calibrations have to account for the non-ideal behavior of garnet and plagioclase. The formulations of NEWTON and HASELTON (1981), HODGES and SPEAR (1982), HODGES and CROWLEY (1985) were used for the calculations (Fig. 8). Each calibration has its own model for plagioclase. The garnet solution model is the same in the calibrations of HODGES and SPEAR (1982) and HODGES and CROWLEY (1985). The obtained pressure ranges of the three GASP calibrations are superimposed on each other with NEWTON and HASELTON (1981) showing a steeper slope in P-T space than the two others.

Figure 8 shows also that the pressure range of the two samples is significantly different. The small overlapping range corresponds to about 7 kbar and 625 °C reflecting well with the conditions of the Alpine amphibolite facies.

Using the calibrations of HODGES and SPEAR (1982) the following average conditions are obtained: The garnet Fe–Mg exchange thermometry yields temperatures that range from 626 to 639 °C in the Simano nappe. The uncertainty of the GARB thermometer is ± 50 °C. The temperatures obtained for the Adula nappe range from 640 to 670 °C. The Ca-exchange barometry yields pressures of 6.0 to 6.3 kbar for the Simano nappe and 7.9 to 8.8 kbar for the Adula nappe. The uncertainty associated with the calibration is ± 500 bar.

4. Discussion and conclusions

The present study provides new data regarding the Adula-Simano nappe boundary and the metamorphic conditions of the studied area.
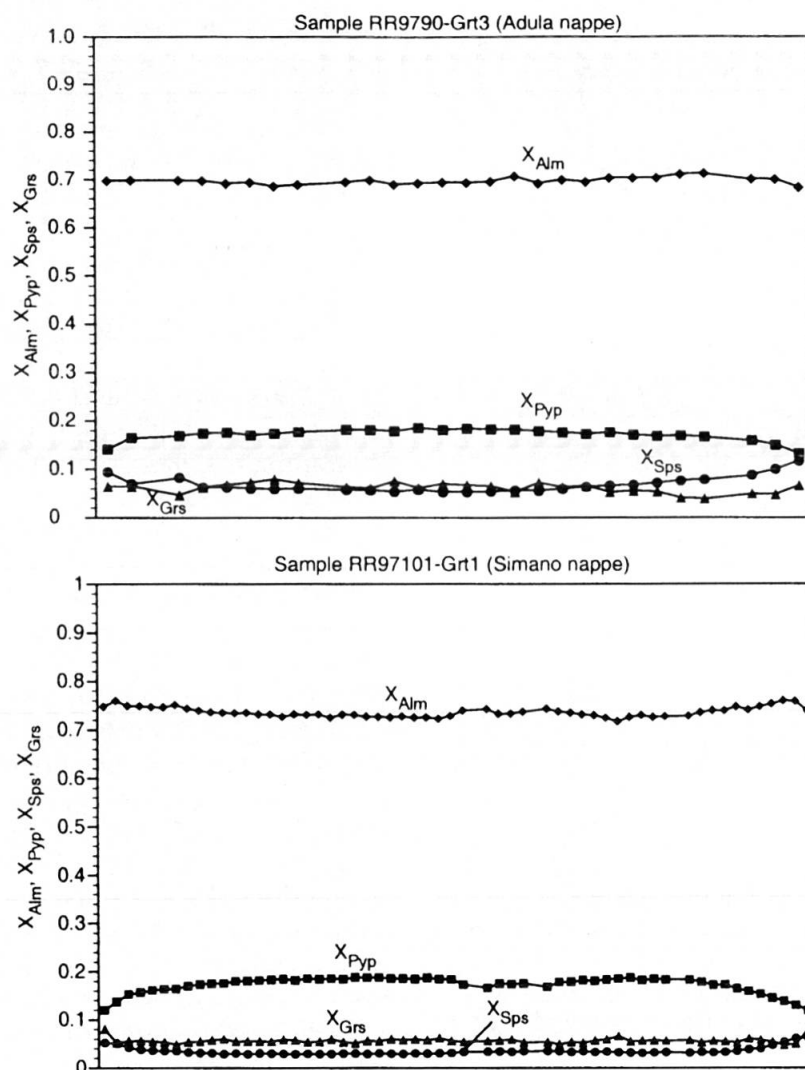
Fig. 7 Garnet profiles measured with the electron microprobe in samples RR97-90 (Adula nappe, 30 measurement points with a spacing of 21μm) and RR97-101 (Simano nappe, 60 measurement points with a spacing of 41μm). The left and right edges of the diagram correspond to the rim of the garnet.

The Adula nappe was thrust onto the Simano nappe by a north-directed movement during D_1. The deformation phase D_2 represents the main phase of Alpine deformation at upper amphibolite facies metamorphic conditions of 7 kbar and 625 °C. The nappe boundary was isoclinally folded during this event (Fig. 3). The structures due to the deformation phase D_2 represent the dominant structures in the entire region. Deformation phase D_3 corresponds to the backfolding of the Alpine nappe pile (e.g. AYRTON and RAMSAY, 1974). This deformation phase is only locally preserved in the field region. The Post-D_3 deformation phase is brittle deformation of the Alpine nappe pile due to movement along the Insubric line under greenschist facies.

The staurolite decomposition reactions and aluminosilicate polymorphs are consistent with the regional Barrovian-type metamorphism (SPEAR,

1993) of the Central Alps (ENGI et al., 1995) in general and the Sillimanite-in isograd of THOMPSON (1976) in particular. Temperatures calculated by thermobarometry accord well with ENGI et al. (1995) (Tab. 2). However, the pressure conditions differ significantly for the Adula nappe relative to the underlying Simano nappe. As the structural evolution of the two units appears to be the same, the difference in pressure conditions in both nappes cannot be related to the evolution of the two units during D_2 and D_3. The thermobarometric data therefore imply that the metapelites of the Adula nappe record to some extent high-pressure subduction zone conditions. This conclusion is supported by SCHMID et al. (1996) who state that the Lepontine equilibration at moderate pressures in the Adula nappe follows, and is intimately related to, the Tertiary high-pressure metamorphic event. MEYRE et al. (1999) describe high-pressure relics in
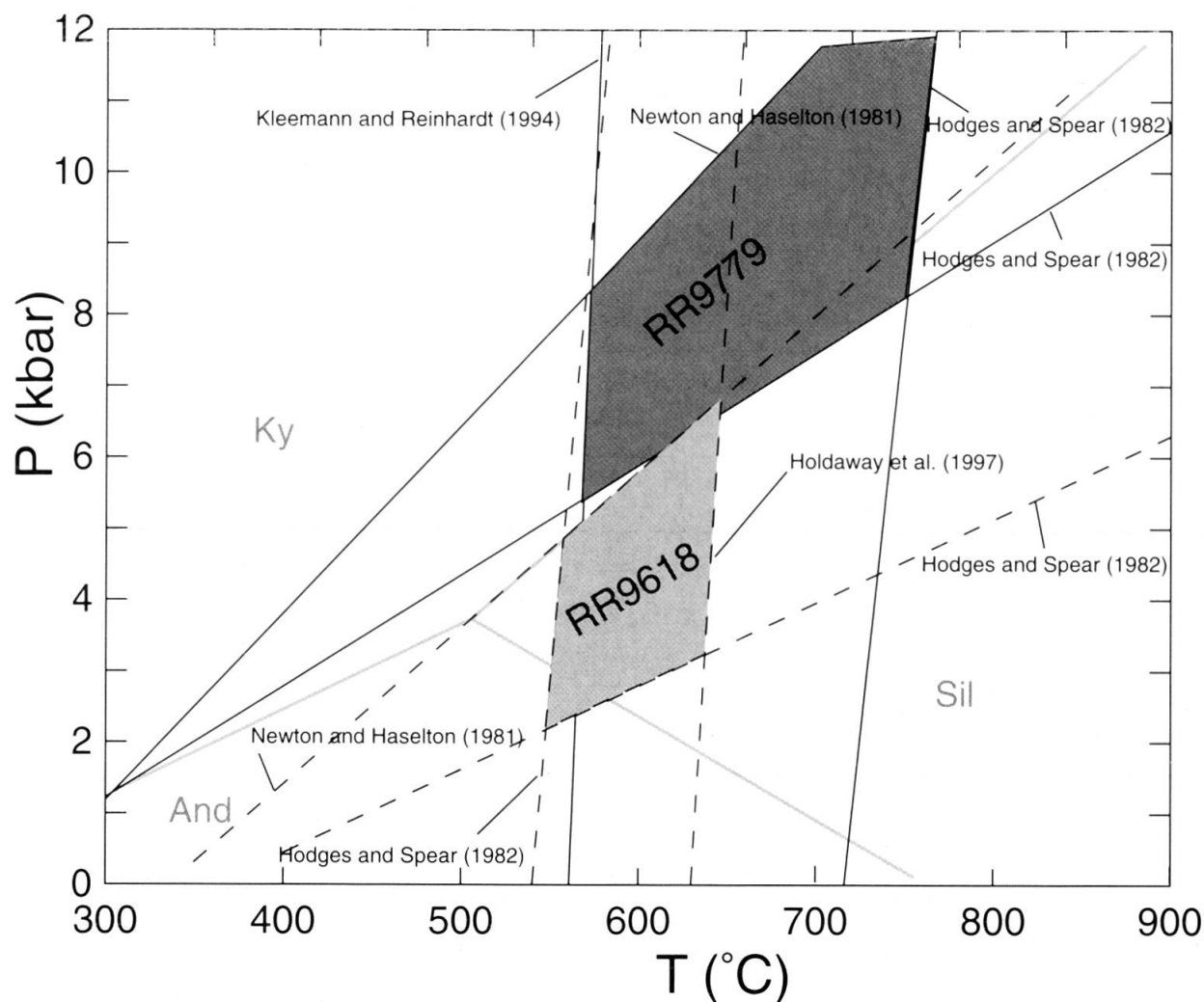
Fig. 8 Graphical results of the thermobarometry on metapelites. The samples represented are RR9618 (Simano nappe) and RR9779 (Adula nappe). The calibrations of HODGES and SPEAR (1982), NEWTON and HASELTON (1981), HODGES and CROWLEY (1985), KLEEMANN and REINHARDT (1994) and HOLDAWAY et al. (1994) are shown, yielding the lowest and highest temperatures and pressures. Further explanation in the text.

metapelites of the middle Adula nappe and conclude that the metapelites of the Adula nappe record the entire structural and petrological retrograde evolution of this Alpine unit.

To date there are no indications for a high-pressure metamorphic event in the lower Penninic Simano nappe although more extensive investigation is necessary to demonstrate this conclusively. Consequently the calculated pressure conditions for the Simano nappe represent the Lepontine Barrovian-type metamorphic conditions of the Central Alps even though pressures from the Simano nappe may have reached 12 kbar (IROUSCHEK, 1983).

The origin of such high-pressure conditions in the Simano nappe and their relation to the exhumation history of the Adula and/or Simano nappe is a subject of ongoing research by the author.

Acknowledgements

References

APPLEGATE, J.D.R. and HODGES, K.V. (1994): Empirical evaluation of solution models for pelitic minerals and their application to thermobarometry. Contrib. Mineral. Petrol., 117, 56–65.

AYRTON, S.N. and RAMSAY, J.G. (1974): Tectonic and metamorphic events in the Alps. Schweiz. Mineral. Petrogr. Mitt., 54, 609–639.

BAUDIN, T., MARQUER, D. and PERSOZ, F. (1993): Basement-cover relationships in the Tambo nappe (Central Alps, Switzerland): geometry, structure and kinematics. J. Struct. Geol., 15, 543–553.

BAUMGARTNER, L. and LÖW, S. (1983): Deformation und Metamorphose der Adula-Decke südwestlich San Bernardino. Schweiz. Mineral. Petrogr. Mitt., 63, 215–232.

BECKER, H. (1993): Garnet peridotite and eclogite Sm–Nd mineral ages from the Lepontine dome (Swiss Alps): New evidence for Eocene high-pressure metamorphism in the Central Alps. Geology, 21, 599–602.

BERMAN, R.G. (1990): Mixing properties of Ca–Mg–Fe–Mn garnets. Amer. Mineral., 75, 328–344.

BIINO, G.G., MARQUER, D. and NUSSBAUM, C. (1997): Alpine and pre-Alpine subduction events in polycyclic basements of the Swiss Alps. Geology, 25, 751–754.

CODONI, A. (1981): Geologia e petrografia della regione del Pizzo di Claro. Unpubl. Ph.D. Thesis, ETH Zürich.

CONNOLLY, J.A.D. (1990): Multivariable phase diagrams: An algorithm based on generalized thermodynamics. Am. J. Sci., 290, 666–718.

DAL VESCO, E. (1953): Genesi e metamorfosi delle rocce basiche e ultrabasiche nell'ambiente mesozonale dell'orogene pennidico. Schweiz. Mineral. Petrogr. Mitt., 33, 173–480.

ENGI, M., TODD, C.S. and SCHMATZ, D.R. (1995): Tertiary metamorphic conditions in the eastern Lepontine Alps. Schweiz. Mineral. Petrogr. Mitt., 75, 347–369.

ERNST, W.G. (1978): Petrochemical study of some lherzolitic rocks from the Western Alps. J. Petrol., 19, 341–392.

ESSENE, E.J. (1989): The current status of thermobarometry in metamorphic rocks. In: DALY, J.S., CLIFF, R.A. and YARDLEY, B.W.D. (eds): Evolution of metamorphic Belts. Geological Society Special Publication, 43, 1–44.

EVANS, B.W. and TROMMSDORFF, V. (1978): Petrogenesis of garnet lherzolite, Cima di Gagnone, Lepontine Alps. Earth Planet. Sci. Lett., 40, 333–348.

EVANS, B.W., TROMMSDORFF, V. and RICHTER, W. (1979): Petrology of an eclogite-metarodingite suite at Cima di Gagnone, Ticino, Switzerland. Amer. Mineral., 64, 15–31.

EVANS, B.W., TROMMSDORFF, V. and GOLES, G. (1981): Geochemistry of high-grade eclogites and metarodingites from the Central Alps. Contrib. Mineral. Petrol., 76, 301–311.

FREY, M., HUNZIKER, J.C., FRANK, W., BOCQUET, J., PIAZ, G.V.D., JÄGER, E. and NIGGLI, E. (1974): Alpine Metamorphism of the Alps. A Review. Schweiz. Mineral. Petrogr. Mitt., 54, 247–290.

FREY, M., JÄGER, E. and NIGGLI, E. (1976): Gesteinsmetamorphose im Bereich der Geotraverse Basel–Chiasso. Schweiz. Mineral. Petrogr. Mitt., 56, 649–659.

FREY, M., BUCHER, K., FRANK, E. and MULLIS, J. (1980): Alpine metamorphism along the Geotraverse Basel–Chiasso – a review. Eclogae geol. Helv., 73, 527–546.

FREY, M., HUNZIKER, J.C., JÄGER, E. and STERN, W.B. (1983): Regional distribution of white K-mica polymorphs and their phengite content in the Central Alps. Contrib. Mineral. Petrol., 83, 185–197.

GEBAUER, D. (1996): A P-T-t path for an (ultra?-) high-pressure ultramafic/mafic rock association and its felsic country rocks based on SHRIMP-dating of magmatic and metamorphic zircon domains. Example: Alpe Arami (Central Alps). In: BASU, A. and HART, S. (eds): Earth Processes: Reading the Isotopic Code. Geophys. Monograph, 95, 307–329.

GRANDJEAN, V., TOTH, T.M. and ENGI, M. (1999): Complex P-T-t history of the Lepontine domain as recorded by garnet-amphibolite from the Simano nappe. J. Conf. Abstracts, 4, 715.

GROND, R., WAHL, F. and PFIFFNER, M. (1995): Mehrphasige alpine Deformation und Metamorphose in der nördlichen Cima-Lunga-Einheit, Zentralalpen (Schweiz). Schweiz. Mineral. Petrogr. Mitt., 75, 371–386.

GRUJIC, D. and MANCKTELOW, N.S. (1996): Structure of the northern Maggia and Lebendun nappes, Central Alps, Switzerland. In: SCHMID, S.M., FREY, M., FROITZHEIM, N., HEILBRONNER, R. and STÜNITZ, H. (eds): Alpine geology; proceedings of the second workshop. Eclogae geol. Helv., 89/1, 461–504.

HEINRICH, C.A. (1986): Eclogite facies regional metamorphism of hydrous mafic rocks in the Central Alpine Adula nappe. J. Petrol., 27, 123–154.

HODGES, K.V. and SPEAR, F.S. (1982): Geothermometry, geobarometry and the Al_2SiO_5 triple point at Mt. Moosilauke, New Hampshire. Amer. Mineral., 67, 1118–1134.

HODGES, K.V. and CROWLEY, P.D. (1985): Error estimation and empirical geothermobarometry for pelitic systems. Amer. Mineral., 70, 702–709.

HOLDAWAY, M.J., MUKHOPADHYAY, B., DYAR, M.D., GUIDOTTI, C.V. and DUTROW, B.L. (1997): Garnet-biotite geothermometry revised: New Margules parameters and a natural specimen data set from Maine. Amer. Mineral., 82, 582–595.

HOLLAND, T.J.B. and POWELL, R. (1998): An internally consistent thermodynamic data set for phases of petrological interest. J. Metamorphic Geol., 16, 309–343.

HUNZIKER, J.C., DESMONS, J. and MARTINOTTI, G. (1989): Alpine thermal evolution in the central and western Alps. In: COWARD, M.P., DIETRICH, D. and PARK, R.G. (eds): Alpine Tectonics. Spec. Publ. Geol. Soc. London, 45, 353–367.

IROUSCHEK, A. (1983): Mineralogie und Petrographie von Metapeliten der Simano-Decke mit besonderer Berücksichtigung cordieritführender Gesteine zwischen Alpe Sponda und Biasca. Unpubl. Ph.D. Thesis, University of Basel.

JENNY, H., FRISCHKNECHT, G. and KOPP, J. (1923): Geologie der Adula. Beitr. Geol. Karte Schweiz, N.F. 51, 123 pp.

KELLER, F. (1968): Mineralparagenesen und Geologie der Campo Tencia-Pizzo Forno-Gebirgsgruppe. Beitr. Geol. Karte Schweiz, N.F. 135, 71 pp.

KLEEMANN, U. and REINHARDT, J. (1994): Garnet-biotite thermometry revisited: The effect of Al^{VI} and Ti in biotite. Eur. J. Mineral., 6, 925–941.

KLEIN, H.H. (1976a): Alumosilikatführende Knauern im Lepontin. Schweiz. Mineral. Petrogr. Mitt., 56, 435–456.

KLEIN, H.H. (1976b): Metamorphose von Peliten zwischen Rheinwaldhorn und Pizzo Paglia (Adula- und Simano-Decke). Schweiz. Mineral. Petrogr. Mitt., 56, 457–479.

KOCH, E. (1982): Mineralogie und plurifazielle Metamorphose der Pelite in der Adula-Decke (Zentralalpen). Unpubl. Ph.D. Thesis, University of Basel.

KORNPROBST, J. (1994): Les roches métamorphiques et leurs signification géodynamique. Précis de pétrologie, Masson, 224 pp.

KRETZ, R. (1983): Symbols for rock-forming minerals. Amer. Mineral., 68, 277–279.

KÜNDIG, E. (1926): Beiträge zur Geologie und Petrographie der Gebirgskette zwischen Val Calanca und Misox. Schweiz. Mineral. Petrogr. Mitt., 6, 1–101.

KUPFERSCHMID, C. (1977): Geologie auf der Lugnezer Seite der Piz-Aul-Gruppe. Eclogae geol. Helv., 70, 1–58.

Löw, S. (1987): Die tektono-metamorphische Entwicklung der nördlichen Adula-Decke (Zentralalpen, Schweiz). Beitr. Geol. Karte Schweiz, N.F. 161, 84 pp.

Marquer, D., Challandes, N. and Baudin, T. (1996): Shear zone patterns and strain distribution at the scale of a Penninic nappe: the Suretta nappe (Eastern Swiss Alps). J. Struct. Geol., 18, 753–764.

Meyre, C. and Puschnig, A.R. (1993): High-pressure metamorphism and deformation at Trescolmen, Adula nappe, Central Alps. Schweiz. Mineral. Petrogr. Mitt., 73, 277–283.

Meyre, C., De Capitani, C. and Partzsch, J.H. (1997): A ternary solid solution model for omphacite and its application to geothermobarometry of eclogites from the middle Adula nappe (Central Alps, Switzerland). J. Metamorphic Geol., 15, 687–700.

Meyre, C., De Capitani, C., Zack, T. and Frey, M. (1999): Petrology of high-pressure metapelites from the Adula nappe (Central Alps, Switzerland). J. Petrol., 40, 199–213.

Möckel, J.R. (1969): Structural petrology of the garnet-peridotite of Alpe Arami (Ticino, Switzerland). Leidse geol. Meded., 42, 61–130.

Mukhopadhyay, B., Basu, S. and Holdaway, M.J. (1993): A discussion of Margules-type formulations for multicomponent solutions with a generalized approach. Geochim. Cosmochim. Acta, 57, 277–283.

Newton, R.C. and Haselton, H.T. (1981): Thermodynamics of the garnet-plagioclase-Al_2SiO_5-quartz geobarometer. In: Newton, R.C., Navrotsky, A. and Wood, B.J. (eds): Thermodynamics of minerals and melts,. Advances in Physical Geochemistry 1, 131–147.

Niggli, P., Preiswerk, H., Grütter, O., Bossard, L. and Kündig, E. (1936): Geologische Beschreibung der Tessiner Alpen zwischen Maggia- und Bleniotal. Beitr. Geol. Karte Schweiz, N.F. 71, 190 pp.

Niggli, E. and Niggli, C.R. (1965): Karten der Verbreitung einiger Mineralien der alpidischen Metamorphose in den Schweizer Alpen (Stilpnomelan, Alkali-Amphibol, Chloritoid, Staurolith, Disthen, Sillimanit). Eclogae geol. Helv., 58, 335–368.

Niida, K. and Green, D.H. (1999): Stability and chemical composition of pargasitic amphiboles in MORB pyrolite under upper mantle conditions. Contrib. Mineral. Petrol., 135, 18–40.

Nimis, P. (1999): Clinopyroxene geobarometry of magmatic rocks; Part 2, Structural geobarometers for basic to acid, tholeiitic and mildly alkaline magmatic systems. Contrib. Mineral. Petrol., 135, 62–74.

Nussbaum, C., Marquer, D. and Biino, G.G. (1998): Two subduction events in a polycyclic basement: Alpine and pre-Alpine high-pressure metamorphism in the Suretta nappe. Swiss Eastern Alps. J. Metamorphic Geol., 16, 591–605.

Partzsch, J.H. (1998): The tectono-metamorphic evolution of the middle Adula nappe, Central Alps, Switzerland. Unpubl. Ph.D. Thesis, University of Basel.

Pfeifer, H.R. (1979): Fluid-Gesteins-Interaktion in metamorphen Ultramafititen der Zentralalpen. Unpubl. Ph.D. Thesis, ETH Zürich.

Pfiffner, M. (1999): Genese der hochdruckmetamorphen ozeanischen Abfolge der Cima Lunga Einheit (Zentralalpen). Unpubl. Ph.D. Thesis, ETH Zürich.

Pouchou, J.L. and Pichoir, F. (1984): Un nouveau modèle de calcul pour la microanalyse quantitative par spectrométrie de rayons X: I. Application à analyse d'echantillons homogènes. Rech. Aérosp., 3, 167–192.

Probst, P. (1980): Die Bündnerschiefer des nördlichen Penninikums zwischen Valser Tal und Passo di San Giacomo. Beitr. Geol. Karte Schweiz, N.F. 153, 63 pp.

Ramsay, J.G. and Huber, M. (1987): The techniques of modern structural analysis. Volume 2: Folds and fractures. Academic Press, 391 pp.

Santini, L. (1993): Geochemistry and geochronology of the basic rocks of the Penninic nappes of East-Central Alps (Switzerland). Unpubl. Ph.D. Thesis, Université de Lausanne.

Schmid, S.M., Pfiffner, O.A., Froitzheim, N., Schönborn, G. and Kissling, E. (1996): Geophysical-geological transect and tectonic evolution of the Swiss-Italien Alps. Tectonics, 15, 1036–1064.

Spear, F.S. and Cheney, J.T. (1989): A petrogenetic grid for pelitic schists in the system SiO_2–Al_2O_3–FeO–MgO–K_2O–H_2O. Contrib. Mineral. Petrol., 101, 149–164.

Spear, F.S. (1993): Metamorphic phase equilibria and pressure-temperature time-paths. Mineralogical Society of America Monograph, Mineralogical Society of America, 799 pp.

Spicher, A., (1980): Tektonische Karte der Schweiz, Schweizerische Geologische Kommission.

Steck, A. and Hunziker, J.C. (1994): The Tertiary structural and thermal evolution of the Central Alps – compressional and extensional structures in an orogenic belt. Tectonophysics, 238, 229–254.

Thompson, P.H. (1976): Isograd pattern and pressure-temperature distribution during regional metamorphism. Contrib. Mineral. Petrol., 57, 277–295.

Todd, C.S. and Engi, M. (1997): Metamorphic field gradients in the Central Alps. J. Metamorphic Geol., 15, 515–530.

Van der Plas, L. (1959): Petrology of the northern Adula region, Switzerland (with particular reference to the glaucophane-bearing rocks). Leidse geol. Meded., 24, 413–603.

Yardley, B.W.D., MacKenzie, W.S. and Guilford C. (1990): Atlas of metamorphic rocks and their textures. Longman Scientific & Technical. 120 pp.